Geomechanics and Engineering, *Vol. 35, No. 5 (2023) 511-523*
https://doi.org/10.12989/gae.2023.35.5.511

The thickness of the soft soil layer and canal-side road failure: A case study in Phra Nakhon Si Ayutthaya province, Thailand

Salisa Chaiyaput*[1], Taweephong Suksawat[2], Lindung Zalbuin Mase[3], Motohiro Sugiyama[4] and Jiratchaya Ayawanna**[5]

[1]*Department of Civil Engineering, School of Engineering, King Mongkut's Institute of Technology Ladkrabang, Bangkok 10520, Thailand*
[2]*Bureau of Testing, Research and Development, Department of Rural Roads, Bangkok 10220, Thailand*
[3]*Department of Civil Engineering, Faculty of Engineering, University of Bengkulu, Bengkulu 38371, Indonesia*
[4]*Department of Civil Engineering, School of Architecture and Urban Planning, Tokai University, Hiratsuka Kanagawa 259-1292, Japan*
[5]*School of Ceramic Engineering, Institute of Engineering, Suranaree University of Technology, Nakhon Ratchasima 30000, Thailand*

(*Received October 23, 2022, Revised November 10, 2023, Accepted November 16, 2023*)

Abstract. Canal-side roads frequently collapse due to an unexpectedly greater soft-clay thickness with a rapid drawdown situation. This causes annually increased repair and reconstruction costs. This paper aims to explore the effect of soft-clay thickness on the failure in the canal-side road in the case study of Phra Nakhon Si Ayutthaya rural road no. 1043 (AY. 1043). Before the actual construction, a field vane shear test was performed to determine the undrained shear strength and identify the thickness of the soft clay at the AY. 1043 area. After establishing the usability of AY. 1043, the resistivity survey method was used to evaluate the thickness of the soft clay layer at the failure zone. The screw driving sounding test was used to evaluate the undrained shear strength for the road structure with a medium-stiff clay layer at the failure zone for applying to the numerical model. This model was simulated to confirm the effect of soft-clay thickness on the failure of the canal-side road. The monitoring and testing results showed the tendency of rapid drawdown failure when the canal-side road was located on > 9 m thick of soft clay with a sensitivity > 4.5. The result indicates that the combination of resistivity survey and field vane shear test can be successfully used to inspect the soft-clay thickness and sensitivity before construction. The preliminary design for preventing failure or improving the stability of the canal-side road should be considered before construction under the critical thickness and sensitivity values of the soft clay.

Keywords: sensitive clay; slope stability; soft clay thickness; rapid drawdown; road collapse

1. Introduction

Landslides are one of the most serious geological hazards, causing thousands of deaths and great property losses per year (Wang and Zhang 2014, Zhang *et al*. 2021, He *et al*. 2022). Canal-side road, a type of infrastructure project, is generally subject to slope failure in landslides. Duncan and Wright (2005) reported that the instability of soil depends on two conditions. One is a reduction in shear strength and another is an increase in the shear stress on the soil as the result of internal factors (e.g., groundwater level), and external factors (e.g., load).

The failure of canal-side roads on soft ground areas occurs annually when the water level in the canal decreases rapidly, which is known as a rapid drawdown (Song *et al.* 2015, Sun *et al*. 2017). The rapid drawdown effect causes a reduction in the safety factor of the canal-side roads. Meanwhile, the opposite side road, under a slow drawdown, does not reduce the safety factor (Hou *et al.* 2021).

The sensitivity of clay is a significant parameter for slope failure (Lundström *et al.* 2009). Viberg (1984) reported that almost all landslides had highly sensitive clay, which had not been clarified before the actual construction. A primary cause of failure is the lack of sufficient soil investigation before construction which has been reported by Jamsawang *et al.* (2021). The severe effect when a failure occurs is not only vital to life but also a budgetary issue for the reparation and stabilization of the canal-side road.

The standard penetration test (SPT), field vane shear test (FVT), and screw driving sounding (SDS) are established soil investigation methods since measuring undrained shear strength (S_u) data can be obtained point by point at the actual location. However, these methods cannot provide the S_u data between each point, and thus, it is difficult to cover a large area on the construction site. These processes, especially the SPT, involve heavy equipment, are time-consuming, and have a high cost for a trial test (Chaiyaput *et al.* 2021, 2022).

Another low-cost nondestructive testing method called "the resistivity survey" was suggested by Godio *et al.* (2006) and Chaiyaput *et al.* (2021). The resistivity survey can present resistivity along with soil thickness through a resistivity contour in a wide area of the subsoil layer under undisturbed conditions (Godio *et al.* 2006). It can also simultaneously identify the weakness zone of canal-side

*Corresponding author, Associate Professor
E-mail: salisa.ch@kmitl.ac.th
**Corresponding author, Associate Professor
E-mail: jiratchaya@sut.ac.th

ISSN: 2005-307X (Print), 2092-6219 (Online)

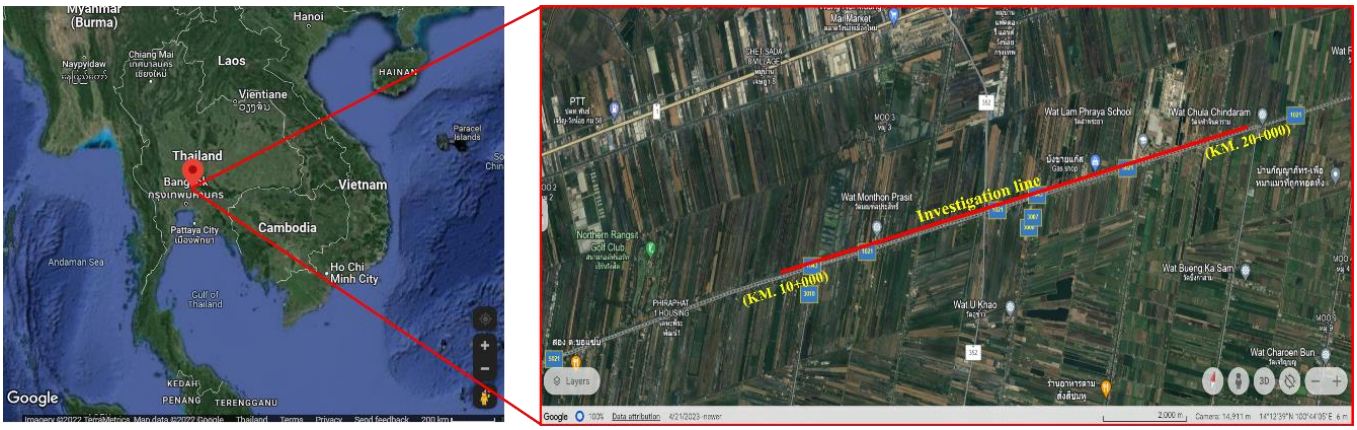

Fig. 1 The location of AY. 1043

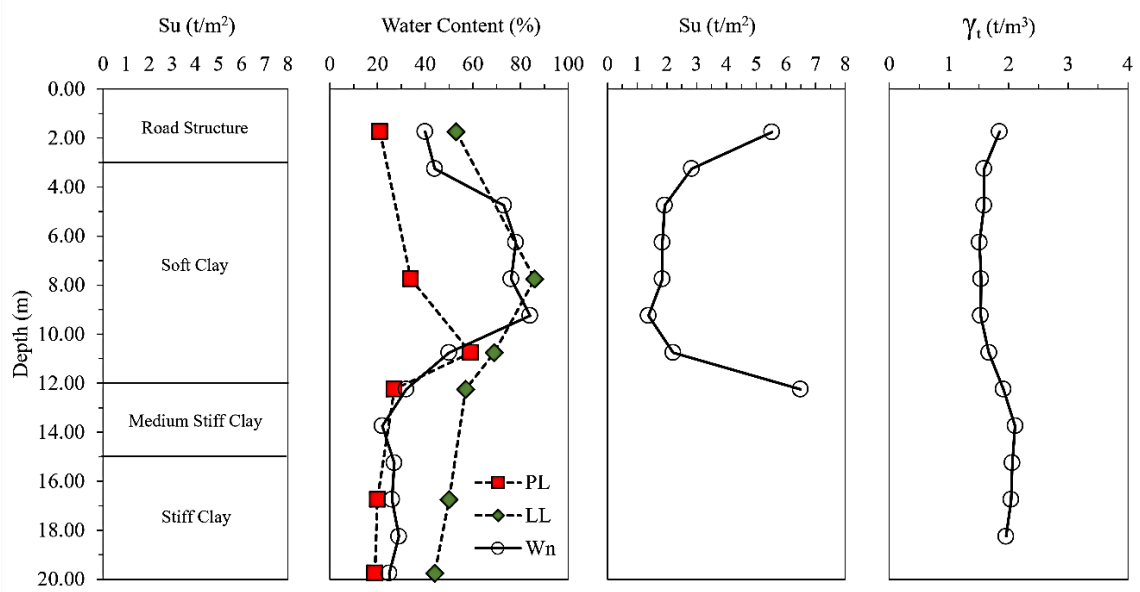

Fig. 2 The properties of subsoil at the AY. 1043

roads and the failure of slopes (Bow 2019). Nevertheless, accurate S_u parameters cannot be obtained from the single use of a resistivity survey. Since only the resistivity survey cannot identify the soil type in each thickness, the FVT or SDS were used to confirm the soil type and consistency of clay by S_u value. The thickness data from the resistivity survey and the S_u value from the FVT and SDS techniques are required to be correlated for the soil investigation.

Therefore, the objective of this research is to investigate the usability of resistivity surveys together with field vane shear tests for the evaluation of unexpectedly greater soft-clay thickness and clay sensitivity related to the failure of canal-side roads. In addition to the suitability of the investigation method, critical conditions, including soil thickness and sensitivity values, are demonstrated for construction engineers. It would be an original work that reveals the new concerning issue accompanied by the preventing model under the critical-thickness and sensitivity values of the soft clay as an innovative model to reduce the potential damage of the canal side road during and after construction.

2. Failure area

The study area is at Phra Nakhon Si Ayutthaya rural road no. 1043 (AY. 1043), Phra Nakhon Si Ayutthaya province, Thailand (Fig. 1). AY. 1043 is located on mangrove swamp deposits, a coastal tide-dominated deposit consisting of clay, silt, and fine-grained sand from tidal flats, marshes, mangrove swamps, and estuaries (Department of Mineral Resources 2021). Fig. 2 shows the subsoil properties at AY. 1043. The subsoil profile under the road structure consisted of three layers, each with different thicknesses; soft clay (9 m), medium stiff clay (3 m), and stiff clay (5 m). The natural water content (W_n) above 10 m depth was comparable to the liquid limit (LL), while the W_n located below the 10 m depth was comparable to the plastic limit (PL). This means that the subsoil above the 10 m depth was in a liquid state, whereas the subsoil located below the 10 m depth was in a plastic state. A field vane shear test was applied to measure S_u of the soft clay layer, which was very low as usual.

Fig. 3 The Failure of Roadways near the Canal Side at AY. 1043

AY. 1043 is a 2-lane asphaltic concrete road having a 6-m wide section and a 1.5-m wide shoulder in each direction. AY. 1043 is a two-way traffic road having a total length of 21.40 km along an irrigation canal on one side of the road. This is called "the canal-side road". The road structure is at a 3-m height consisting of a side slope with a vertical-to-horizontal ratio of 1:1.5 (1V:1.5H). The canal is located at a depth of about 6 m below the pavement surface or 3 m below the ground surface. The failure areas at KM. 16+720, KM. 18+060, and KM. 18+570 were found after the water level in the canal continually dropped until it was almost dried up as shown in Fig. 3.

3. Site Investigations

3.1 Numerical simulation procedure

3.1.1 Field vane shear test

The field vane shear test (FVT) corresponding to the ASTM D-2573 is a common in-situ method to investigate the S_u of subsoil in a target area. The clay consistency can be identified by S_u values under the ASTM D-2488 to be a very soft clay (S_u = 0-13 kPa), a soft clay (S_u = 13-25 kPa), a medium-stiff clay (S_u = 25-50 kPa), a stiff clay (S_u = 50-100 kPa), a very stiff clay (S_u = 100-200 kPa), a hard clay (S_u = 200-400 kPa), and a very hard clay (S_u > 400 kPa). The FVT was performed by the Department of Rural Roads, Thailand before the construction of AY. 1043 began. The FVT procedures and calculations were reported in previous work (Chaiyaput *et al.* 2021). Moreover, the S_u from FVT ($S_{u\ (FVT)}$) procedures were corrected with the correction factor (μ) derived from the equation: $S_u = \mu S_{u\ (FVT)}$, which was proposed by Bjerrum (1972).

The FVT was carried out at the following 26 locations: KM. 10+220, KM. 10+320, KM. 10+600, KM. 10+820, KM. 14+200, KM. 14+400, KM. 14+600, KM. 16+650, KM. 16+700, KM. 17+600, KM. 17+750, KM. 17+820, KM. 18+000, KM. 18+140, KM. 18+240, KM. 18+350, KM. 18+430, KM. 18+500, KM. 18+610, KM. 18+730, KM. 18+830, KM. 18+950, KM. 19+060, KM. 19+400, KM. 19+500, and KM. 19+600. The FVT was restricted at the depth of the medium stiff clay, and therefore the FVT was carried out until the end of the soft soil layer. The S_u at non-failure locations (KM. 10+600 and KM. 14+400) and failure locations (KM. 16+700, KM. 18+350, and KM. 18+500) were subsequently compared to analyze the thickness of soft clay at the non-failure locations and failure locations as shown Fig. 4.

From the above locations, the thickness of the soft clay layer at the non-failure areas was about 6 m (measuring from 3 m to 9 m depth below the pavement surface) at KM. 10+600 and 9 m (measuring from 3 m to 12 m depth below the pavement surface) at KM. 14+400. Meanwhile, the thickness of the soft clay layer at the failure locations was about 10 m (measuring from 3 m to 13 m depth below the pavement surface) at KM. 16+700, 11 m (measuring from 3 m to 14 m depth below the pavement surface) at KM. 18+350, and 12 m (measuring from 3 m to 15 m depth below the pavement surface) at KM. 18+500.

The thickness of the soft clay layer at the 26-testing locations, which covered the 3-failure locations (KM. 16+720, KM. 18+060, and KM. 18+570), was summarized and plotted as shown in Fig. 5. The road structure was 3 m-height, and thus the ground surface was presented at the bottom of the road structure as a dashed line. The thickness of the soft clay varied from 1 m to 12 m below the dashed line. As shown in Fig. 5, the thickness of the soft clay layer at the failure locations was higher than that of the non-failure locations. The total thickness of the soft clay was over 9 m at the failure locations, whereas the thickness of the soft clay at the non-failure locations was less than 9 m. This result suggests that the higher thickness of the soft clay the higher risk of the failure found at the canal-side road located on the soft clay layer.

3.1.2 Soil sensitivity

The sensitivity of clay is defined as the ratio of the S_u in an undisturbed state to the S_u in a remolded state, which was investigated by FVT before the construction of AY. 1043 began. The strength for both states was determined by the same moisture content. The sensitivity value is considered to be insensitive when the value < 2. Sensitive values are in the range of 4 – 8. Extra sensitive values are considered to be 8 – 16, while a sensitivity value > 16 is referred to as quick clays

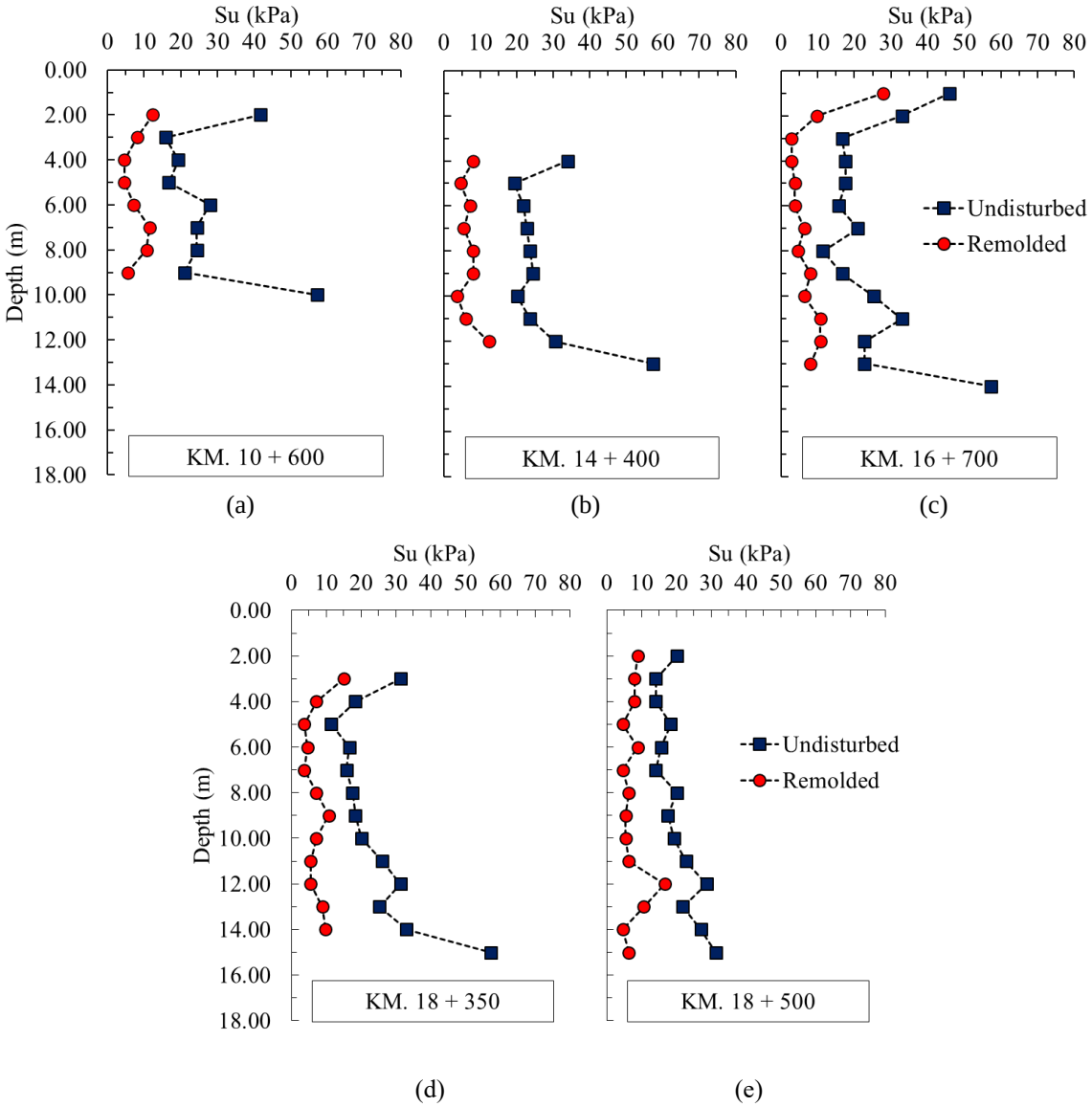

Fig. 4 FVT results before the construction of AY. 1043 began (a) KM. 10+600, (b) KM. 14+400, (c) KM. 16+700, (d) KM. 18+350, and (e) KM. 18+500

(New Zealand Geotechnical Society 2005). The calculated sensitivity from the results of the field vane shear test is shown in Fig. 6. The sensitivity values were determined to be between 1.96 to 4.18 at KM. 10+600, 1.49 to 4.21 at KM. 14+400, 1.65 to 6.07 at KM. 16+700, 1.73 to 5.72 at KM. 18+350, and 1.72 to 5.86 at KM. 18+500. That means the sensitivity values < 4.5 appeared at the non-failure locations at KM. 10+600 and KM. 14+400. Meanwhile, the sensitivity values > 4.5 appeared at the failure locations at KM. 16+700, KM. 18+350, and KM. 18+500.

3.2 Soil investigation after the canal-side road failure

3.2.1 Resistivity survey

A resistivity survey was conducted to perform geophysical mapping and to evaluate the thickness of the soft clay layers at the failure area (KM. 16+720, KM. 18+060, and KM. 18+570). Normally, igneous and metamorphic rocks have high resistivity values compared to soil and water, which have low resistivity values. Moreover, the soil properties i.e., mineral content, organic content, fluid content, porosity, water content, temperature, and dissolved salt, have an influence on the fluctuation of electrical resistivity values (Prabhakar and Deshpande 2014, Loke and Barker 1996a, b). Thus, the electrical-resistivity tomography from the resistivity survey can identify soil types based on the unified soil classification system (USCS) at different depths (Kaufman and Hoekstra 2001) and can evaluate the weakness point at the failure area.

In the resistivity survey, resistivity (ρ) with the unit of Ωm is calculated based on the theoretical relationship between the electric field (E; V/m) and the current density(J; A/m^2) as shown in Eq. (1)

$$\rho = E/J \qquad \text{(Ohm·metres, Ωm)} \qquad (1)$$

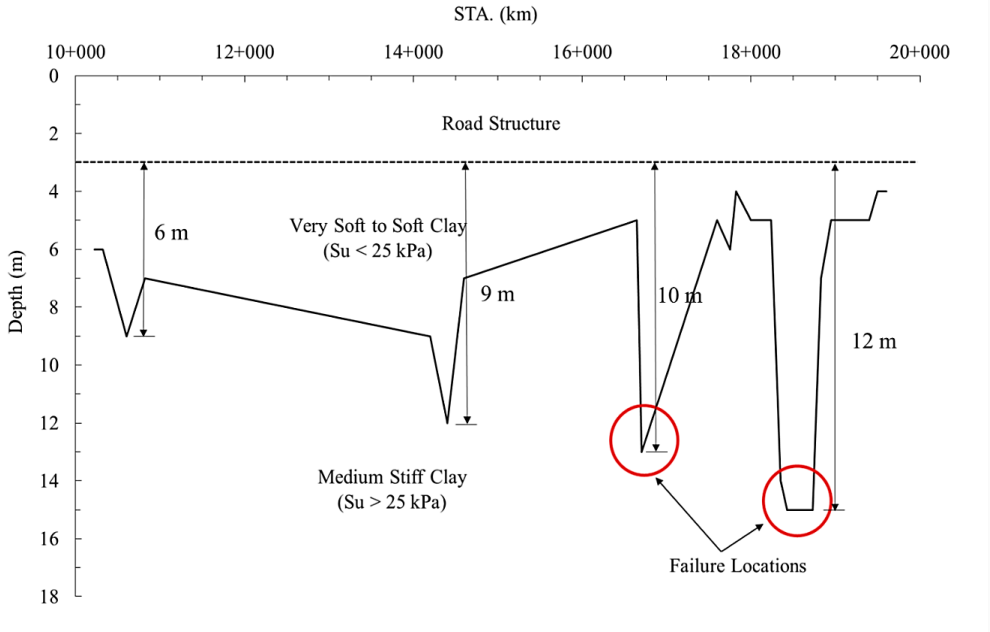

Fig. 5 The thickness of the soft clay layer at 26-testing locations of AY. 1043

However, the resistivity obtained by a field survey is usually an apparent resistivity. The measured apparent resistivity (ρ_a) is determined by Eq. (2).

$$\rho_a = \frac{k\Delta V}{I} \tag{2}$$

where I = injecting current at the point source. The differential potential (ΔV) between electrodes M and N is determined by Eq. (3) and the Geometric factor (k) is determined through Eq. (4), respectively.

$$\Delta V = \frac{\rho I}{2\pi}\left\{\left(\frac{1}{r_1}-\frac{1}{r_2}\right)-\left(\frac{1}{r_3}-\frac{1}{r_4}\right)\right\} \tag{3}$$

$$k = \frac{2\pi}{\left\{\left(\frac{1}{r_1}-\frac{1}{r_2}\right)-\left(\frac{1}{r_3}-\frac{1}{r_4}\right)\right\}} \tag{4}$$

For multiple-gradient arrays; $r_1 = na$, $r_2 = (n+1)a$, $r_3 = (s+2-n)a$, $r_4 = (s+1-n)a$.

According to the diagram in Fig. 7(a), the electrode configuration of multiple gradient arrays shows the injecting current electrodes between A and B, which are fixed at the end of the survey line. Meanwhile, the measuring potential electrodes between M and N can be moved within the injecting current electrode at any interval of the minimum electrode spacing. The position of the electrodes for measurement by injecting current electrodes is separated by $(s+2)a$, where a is the minimum spacing between the potential electrodes and s is the separation factor (Dahlin and Zhou 2006).

The resistivity survey with the multiple-gradient arrays is thus carried out by measuring the potential differences between the potential electrodes (M-N) sequentially with spacing a. The parameter n is the relative spacing between the potential dipole and the closest current electrode. The n parameter is also defined as a vector, which is positive at higher coordinates and negative at lower coordinates test (Chaiyaput *et al*. 2022).

The failure area at KM. 16+720, KM. 18+060, and KM. 18+570 located on the AY. 1043 were investigated using a resistivity survey with multiple gradient arrays that provide very stable field-data acquisition and significantly increase the speed of data acquisition with a good signal-to-noise ratio (Dahlin and Zhou 2006). The resistivity survey was conducted with a single line in the longitudinal profile, covering the entire length of the failure area, as shown in Fig. 7.

The measured apparent resistivity data with pseudo depth in geophysical mapping was inverted to a resistivity model section of the inverted resistivity *vs.* depth that can be used for subsurface geological interpretation. The variations of the inverted electrical resistivity (ρ) were presented with various depths at 3 different failure locations: KM. 16+720 (Fig. 8(a)), KM. 18+060 (Fig. 8(b)), and KM. 18+570 (Fig. 8c). According to the results of the resistivity survey in Fig. 8, the ρ from all failure locations showed a similar variation of ρ, which can be classified into 2 types of soil. High ρ values in the range of 4.5 – 9.0 Ω m were detected at the top layer (from the pavement surface to 3 m depth below the pavement surface) of the canal-side road. Conversely, low ρ values in the range of 1.5 – 4.5 Ω m were found below 3 m depth from the pavement surface.

This result suggests that the strongest materials exist on the top layer of the road structure of the canal-side road which supports heavy loads and transmits high stresses. It corresponds to the general geometry of the canal-side road containing asphalt concrete, crushed rock, lateritic soil, and selected materials from the top layer to the bottom layer, respectively. Meanwhile, the variation of ρ values from 3 m to 14 m depth below the pavement surface was in the range

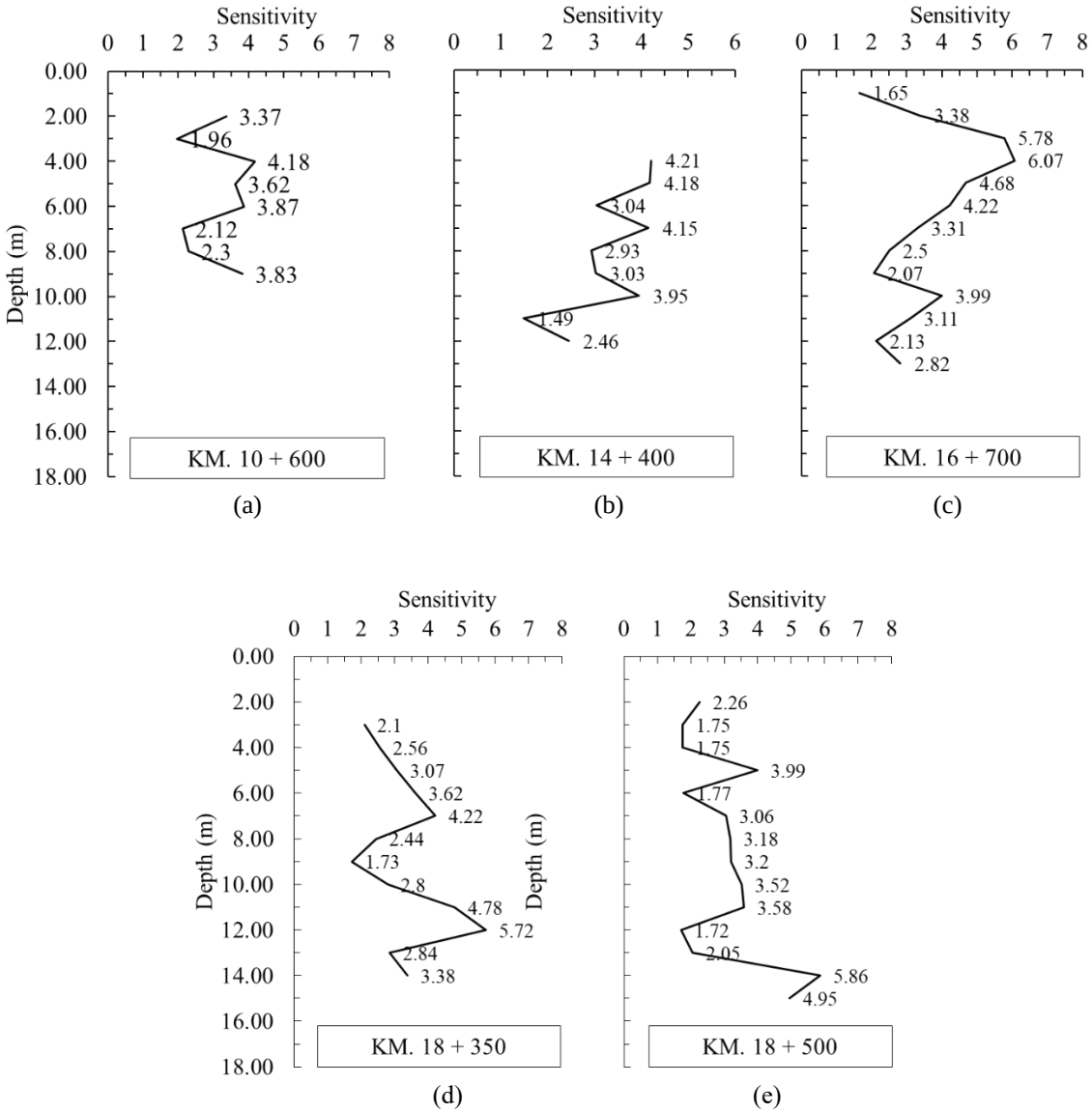

Fig. 6 Sensitivity of subsoil at AY. 1043 (a) KM. 10+600, (b) KM. 14+400, (c) KM. 16+700, (d) KM. 18+350, and (e) KM. 18+500

of 1.5 – 4.5 Ωm, which is a low resistivity value. This thickness range corresponds to the soft clay layer from the FVT mapping in Fig. 5. Moreover, this result agrees with the report from Kaufman and Hoekstra (2001) with a low ρ value for fine soil particle sizes. The results of the resistivity survey are also related to the results of S_u from FVT and SDS (Chaiyaput *et al*. 2022).

3.2.2 Screw driving sounding test

Screw driving sounding (SDS) was used to determine the S_u of subsoil. The working diagram of SDS was shown in Fig. 9. The SDS method is a new in-situ method with a simpler system, faster procedure, and more economical test compared with other tests (Orense *et al.* 2019). Moreover, the SDS method reveals the capability to determine S_u at deeper subsoil layers compared with the FVT method. The SDS test was applied to the AY. 1043 road at the KM. 16+720, KM. 18+060, and KM. 18+570 to determine the S_u after failure took place. The S_u data from the SDS test was used to confirm the depth of the soft soil layer at those 3-failure locations. The process of the SDS was explained in the previous work (Chaiyaput *et al.* 2021).

The relationship between the S_u from SDS tests and the depths of 3-failure locations is shown in Fig. 10. The measured S_u was demonstrated by 4-depth zones according to the different tendencies of S_u. Depth zone 1 was measured from the pavement surface to 3 m depth below the pavement surface. In this zone, the S_u fluctuated highly from 7.5 kPa to 70 kPa because of the various strengths of the materials in the road structure at each location. Meanwhile, the distribution of S_u at the depth zones 2 and 3 was relatively similar among all 3-failure locations.

The tendency of S_u was slightly increased with an increase in depth. Depth zone 2 ranging from 3 m to 9 m in

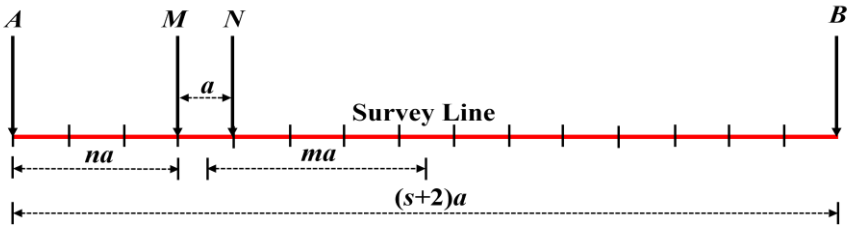

(a)

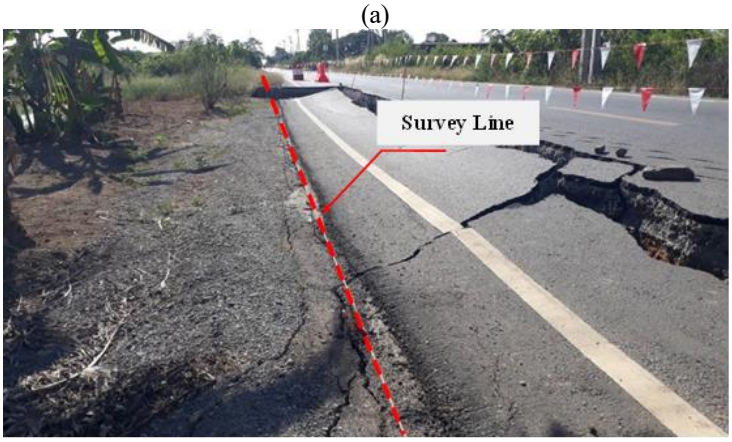

(b)

Fig. 7 (a) Electrode configuration of resistivity survey (b) resistivity survey profile at the failure area on the AY. 1043

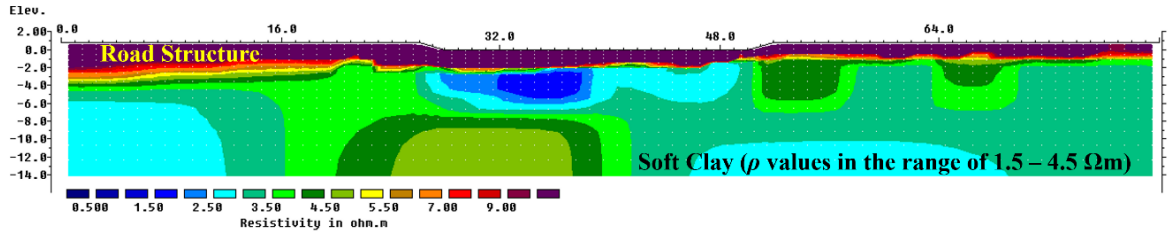

(a) KM. 16+720

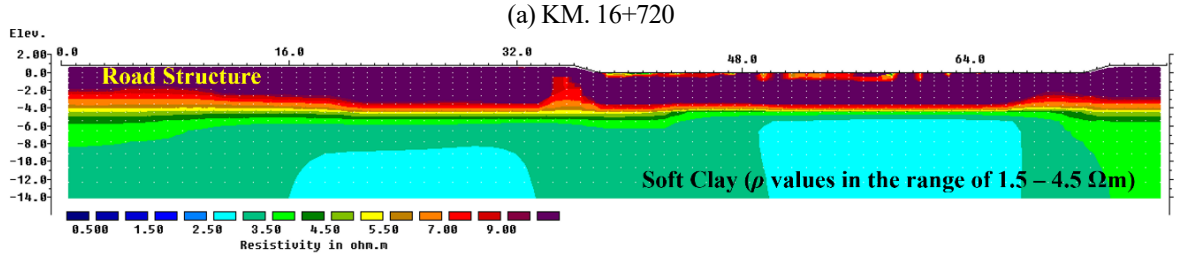

(b) KM. 18+060

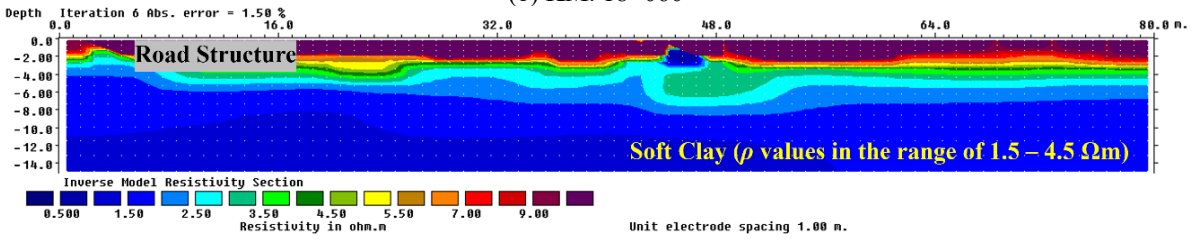

(c) KM. 18+570

Fig. 8 The variations of ρ with various depths of the canal-side road at 3-different failure locations (a) KM. 16+720, (b) KM. 18+060, and (c) KM. 18+570

depth below the pavement surface exhibited a S_u distribution in the range of 13 kPa to 30 kPa. Depth zone 3 ranging from 9 m to 12 m in depth below the pavement surface exhibited a S_u distribution in the range of 25 kPa to 35 kPa. Meanwhile, the S_u distribution at depth zone 4 (depth of over 12 m below the pavement surface) broadly ranged from 30 kPa to 75 kPa. According to ASTM D-2488, the S_u value at depth zone 2 belongs to that of soft

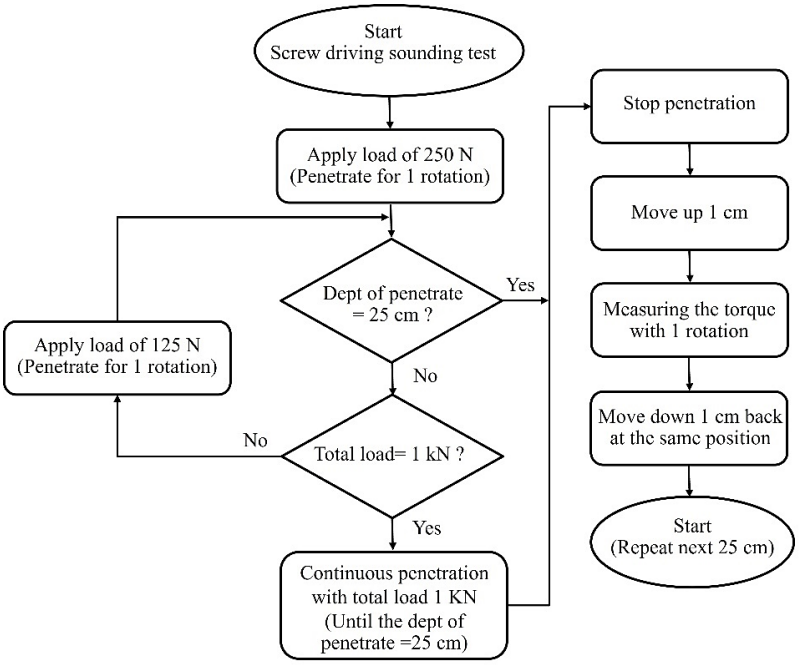

Fig. 9 Working diagram of SDS

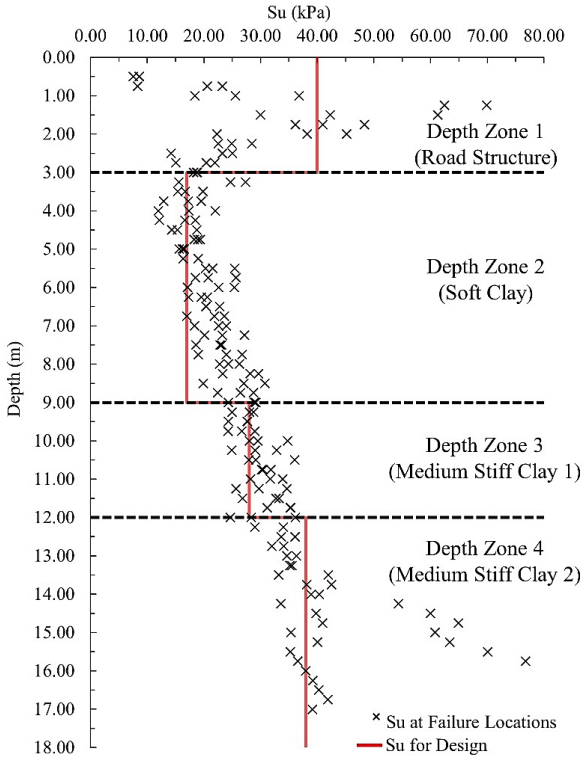

Fig. 10 S_u from SDS test at failure locations

clay, whereas S_u values at depth zones 3 and 4 correspond to medium-stiff clay with a bit higher stiffness at depth zone 4.

The S_u from the SDS test was considered a design parameter for the numerical simulation to understand the effect of soft clay thickness on canal-side road failure. According to the red line in Fig. 10, the S_u distribution of subsoil at depths of 0 m to 3 m below the pavement surface (depth zone 1) belonging to the road structure has high fluctuation. The S_u was thus approximated in the middle of the fluctuated-S_u data to be ~40 kPa for further numerical simulation. Meanwhile, the other zones of S_u distribution were estimated from the low region of distribution, which spread of S_u data remains in line with depth and follows ASTM D-2488. Hence, further numerical simulation was

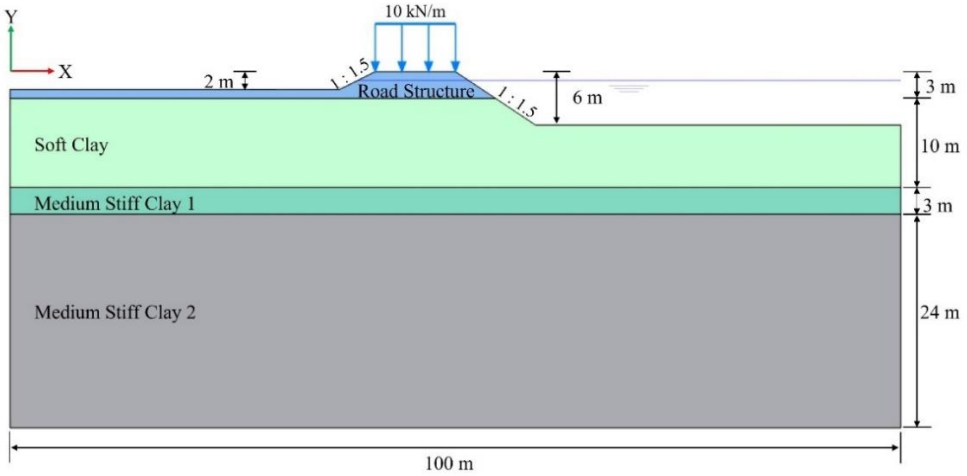

Fig. 11 FEM model of the failure location

Table 1 Parameters used in FEM

Materials	Thickness	Model	Material	γ_{sat}	γ_{unsat}	$k_x = k_y$	E'	ν'	λ^*	κ^*	S_u	$\emptyset$
	(m)		behavior	(kN/m^3)		(m/day)	(kPa)				(kPa)	(˚)
Road structure	3	MCM	D	18	16	2×10^{-3}	8000	0.30			40	5
Soft clay	6 and 10	SSM	U	16	15	8×10^{-4}		0.495	0.1	0.009	15	1
Medium Stiff clay 1	3	MCM	U	18	16	4×10^{-4}	5000	0.33			28	0
Medium Stiff clay 2	24	MCM	U	19	17	4×10^{-4}	7500	0.33			40	0

MCM: Mohr-Coulomb Model, SSM: Soft-Soil Model, D: Drained, U: Undrained

subjected to ~15 kPa S_u at 3 m to 9 m depth below the pavement surface (depth zone 2), ~28 kPa S_u at 9 m to 12 m depth below the pavement surface (depth zone 3), and~40 kPa S_u at > 12 m depth below the pavement surface (depth zone 4), respectively.

4. Numerical simulation

The numerical simulation through the finite element method (FEM) was employed to analyze the stability of the canal-side road. The two-dimensional (2D) software with the plane strain (2D) condition was suitable for the geometry of the canal-side road and slope (Latha and Garaga 2010, Bergado *et al.* 2017, Udomchai *et al.* 2018, Chaiyaput and Bergado 2018, Tran *et al.* 2019, Chaiyaput *et al.* 2014, 2021). The stability of the canal-side road can primarily be assessed by the factor of safety (*FS)* against global failure (FS_{global}). This is a very useful index to find out how close or far the canal-side road is from failure according to the study by Rao *et al.* (2021). The canal-side road is considered to be stable when the *FS* is more than 1 and the resisting shear strength is greater than the driving shear stress. The 2D-FEM software was allowed to calculate FS_{global} based on the phi-c reduction method as described in the previous work (Artidteang *et al.* 2013, Chaiyaput *et al*. 2012, 2014, 2021).

With the present analysis conditions, the 2D-FEM licensed software (PLAXIS 2-D version 20.04.00.790 supported by the Department of Rural Roads) was carried out on the canal-side road for calculations based on the phi-c reduction method. This aims to consider the stability at the non-failure locations and the failure locations due to variations in the soft clay thickness underneath the canal-side road section as shown in Fig. 5. The 6-m thick and 10-m thick, soft clay layers from Fig. 5 were compared to evaluate the effect of soft clay thickness on canal-side road failure as one of the analysis conditions. Moreover, the water level in the canal is another important consideration for the analysis of conditions of road failure, especially rapid drawdown conditions.

4.1 Canal-side road modeling and parameters

The soil profile from the resistivity survey was successfully mapped with the shear strength parameter from the SDS test Chaiyaput *et al.* (2021). Therefore, the investigation data from the field test were used to create and model the thickness of the soft clay layer, and the geometrical of the canal-side road at the non-failure and failure locations as shown in Fig. 11. The typical geometry of the canal-side road and subsoil at AY. 1043 was modeled within 100 m width on the x-axis and 40 m depth on the y-axis, which was enough to avoid any boundary effects. For the boundary conditions, the bottom and the surface of the FEM model were assigned as fixed boundary and free boundary, respectively, while the sides of the FEM model were assigned as the roller boundaries.

The model of the road structure was 9 m wide, which consisted of 6 m wide for traffic lanes in 2 directions and 1.5 m

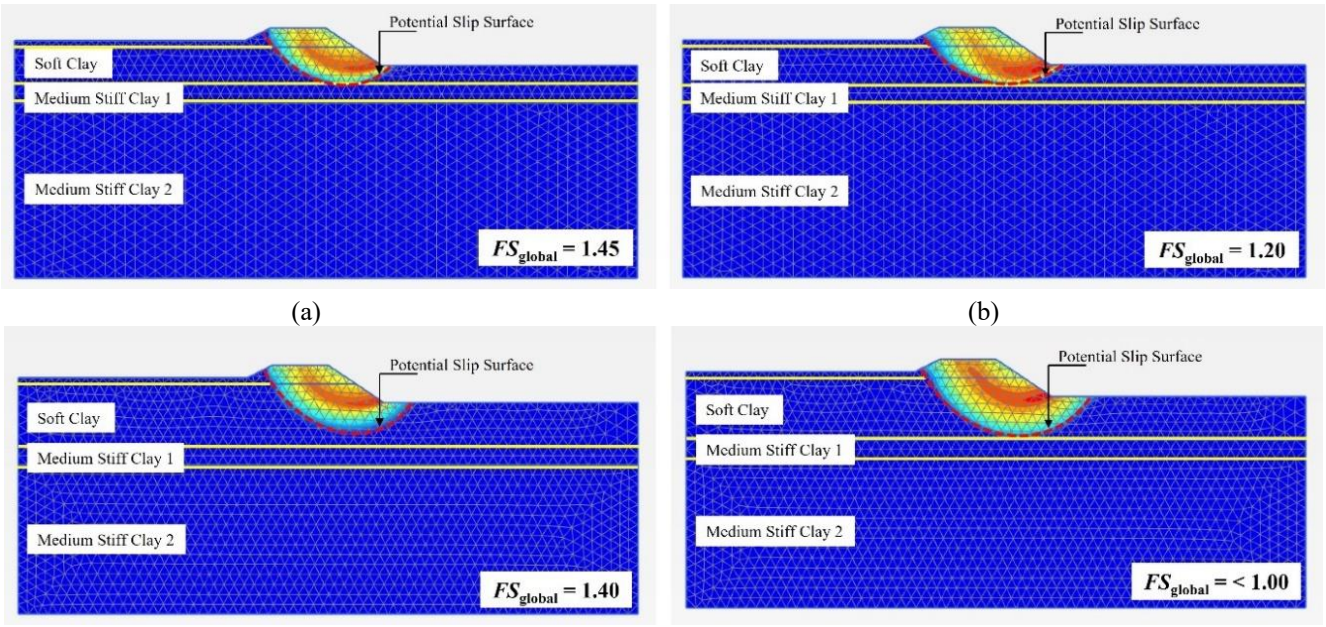

Fig. 12 The factor of safety at (a) 6 m thick of soft clay layer with the water level at -1 m below pavement surface, (b) 6 m thick of soft clay layer with the water level at -4 m below pavement surface, (c) 10 m thick of soft clay layer with the water level at -1 m below pavement surface and (d) 10 m thick of soft clay layer with the water level at -4 m below the pavement surface

wide for the shoulder of each side. The side slope is 1V:1.5H (Vertical: Horizontal). The depth of the canal is about 6 m depth below the pavement surface. The traffic load (10 kN/m) was simulated on the surface of the road structure as shown in Fig. 11. The subsoil model was divided into four layers. The first layer was the 3 m thick (S_u = 40 kPa) road structure followed by a soft clay as a second layer (S_u = 15 kPa). The third layer was a layer of medium stiff clay 1 with a thickness of 3 m (S_u = 28 kPa). The fourth layer was the medium-stiff clay 2 (S_u = 40 kPa). The soil parameters (Table 1) were assigned to the FEM model under drained conditions (for road structures) and undrained conditions (for soft clay and medium-stiff clay). A Mohr-Coulomb model with a strengthparameter was used for the road structure and the medium-stiff clay. Meanwhile, the soft soil model is one of the clay models, which is suitable for materials with high degrees of compressibility, such as normally consolidated clay used for the soft clay in the present work.

The strength parameter, which was S_u, was obtained from the SDS test (Fig. 10). Other soil parameters (saturated unit weight (γ_{sat}), unsaturated unit weight (γ_{unsat}), horizontal permeability (k_x), horizontal permeability of 90° (k_y), and elasticity (E')) were based on the studies of Likitlersuang *et al.* (2013) and Chaiyaput *et al.* (2014). The upper layer was the road structure (from the pavement surface to 3 m depth below the pavement surface).

The analyzing parameters were performed using the following values, Poisson's ratio (v') = 0.30 and an elasticity (E') = 8000 kPa. The S_u was obtained from the SDS test by using strength parameters = 40 kPa and friction angle of (ϕ') = 5°. The soft clay layer found under the road structure was modeled for 6 m and 10 m depths below the pavement surface. The soft-soil model with an undrained condition was applied with S_u = 15 kPa and ϕ' = 1°. Additional values for analysis were modified using a compression index (λ*) = 0.10 and a modified swelling index (κ*) = 0.009. The medium-stiff clay layer was divided into a medium-stiff clay layer 1 and a medium-stiff clay layer 2. The medium-stiff clay layer 1 was under the soft clay layer with a thickness of 3 m. The Mohr-Coulomb model with undrained behavior was assigned values of v' = 0.33, S_u = 28 kPa, and E' = 5,000 kPa. Meanwhile, the medium-stiff clay layer 2, which is the final layer of the FEM model used the analyzing values of v' = 0.33, S_u = 40 kPa, and the E' = 7,500 kPa.

Due to variations in the thickness of the soft-clay layer underneath the section of the canal-side road (Fig. 5), the model of soft clay at 6 m thick (non-failure location) and 10 m thick (failure location) were compared. Then, the effect of soft-clay thickness on the FS_{global} of the canal-side road was determined by varying the water level in the canal at depths of -1 m and -4 m below the pavement surface to simulate the behavior of canal-side road failure due to full water level and rapid drawdown conditions, respectively.

The rapid drawdown condition means the fast reduction of water level occurred in the canal. The high pore-water pressure remains inside the road structure. The water level at -4 m depth below the pavement surface was simulated by a decrease of water level in the canal from depths of -1 m to -4 m below the pavement surface within a 9-day period under the transient groundwater flow calculation.

The deformed mesh of 10 m thick of soft clay was observed relating to the deformation of road structure after simulation with the decreasing water level at -4 m below the pavement surface. This suggests that during rapid drawdown, the restraining water force is removed. An

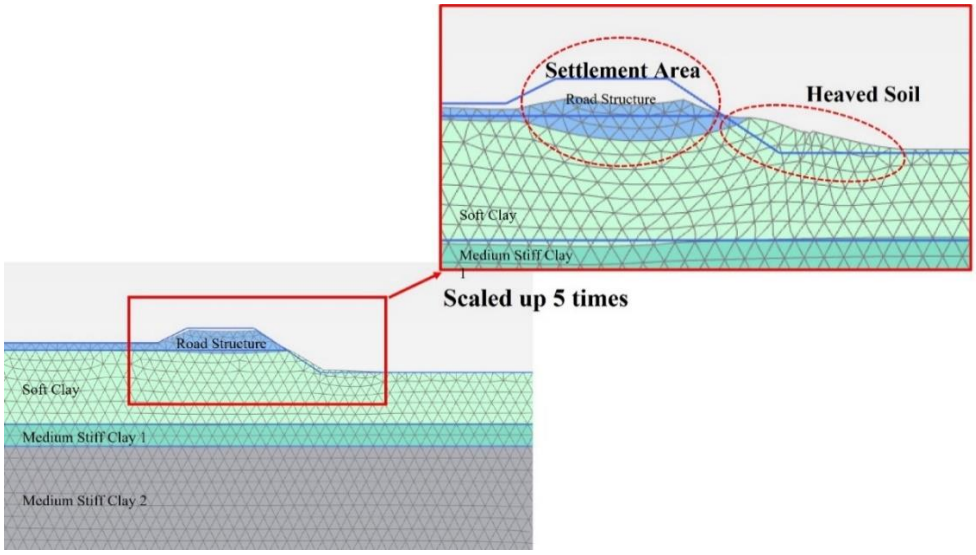

Fig. 13 The deformed mesh of 10 m thick of soft clay layer with a water level at -4 m below the pavement surface

excess pore-water pressure cannot dissipate, resulting in the settlement of road structure and heaved soil, as shown in Fig. 13.

4.2 Simulation results and discussion

The FS_{global} of the natural slope is considered between 1.25 and 1.40 (Neoh 2009). From Fig. 12, the highest FS_{global} value of 1.45 was obtained at a soft-clay thickness of 6 m with a water level of -1 m depth below the pavement surface (Fig. 12(a)). Meanwhile, the FS_{global} value of 1.20 was obtained at a soft-clay thickness of 6 m with a water level of -4 m depth below the pavement surface (Fig. 12(b)). Considering the thickness of the soft clay layer of 10 m, the FS_{global} value was 1.40 under the water level of -1 m, and the $FS_{global} < 1.00$ under the water level of -4 m. When the thickness of soft clay increases from 6 m to 10 m, the FS_{global} value decreased from 1.45 to 1.40 under the water level in the canal at -1 m depth below the pavement surface and decreased from 1.20 to < 1.00 under the water level in the canal at -4 m depth below the pavement surface. In the case where the FS_{global} value < 1.00, the calculation of stability was not allowed because the soil body collapsed as shown in Figs. 12(d) and 13.

The above simulation result demonstrates that the thickness of the soft clay layer significantly affected the FS_{global} and potential slip surface, especially in the rapid drawdown condition (the water level in the canal at -4 m depth below the pavement surface). The FS_{global} decreased with an increase in the soft-clay thickness. Moreover, the FS_{global} significantly decreased with a decrease in the water level in the canal (Hou *et al*. 2021). In a rapid drawdown condition, the pore water in the road structure cannot suddenly drain into the canal. The phreatic surface in the road structure becomes higher than the water level in the canal, resulting in transient seepage flowing out of the road structure.

Fig. 13 shows a deformed mesh scaled up 5 times from the canal-side road model. This canal-side road model is composed of 10 m thick-soft clay under a water level of -4 m depth below the pavement surface. The numerical results of the studied model show the destruction of soil bodies. The road structure collapses downwards in the soft clay layer resulting in a heave of the soft clay at the base of the canal. This was similar to the canal-side road conditions at the real-failure location.

The numerical results also confirm that the failure of the canal-side road was caused by an unexpectedly greater thickness of soft clay with a lower water level. According to the field investigation before the start of the construction by field vane shear test, a cause of canal-side road failure compared with non-failure locations was the existence of soft clay over 9 m-thick with sensitivity values > 4.5, which is referred to sensitive clays (New Zealand Geotechnical Society 2005). Thus, precautions should be taken to prevent the destruction of the canal-side roads due to rapid drawdown (Abramson *et al.* 2002), especially with a soft clay layer over 9 m thick.

5. Conclusions

This paper focused on the sensitivity index and the thickness of the soft clay layer, which are significant parameters for canal-side road failures. From the results of this study, the following conclusions can be made:

(1) Canal-side road failure due to soft clay thickness was evaluated through the combination of resistivity survey and field vane shear.

(2) The geophysical mapping combined with the Su results demonstrated critical conditions for the initial failure of the canal-side road, which is located on > 9 m-thick of the soft-clay layer under rapid drawdown conditions with a sensitivity > 4.5.

(3) The 2D-FEM numerical simulation indicated that the thickness of the soft clay layer affected the FS_{global} and a potential slip surface under rapid drawdown conditions and confirmed the significant effect of soft clay thickness on canal-side road failures.

(4) Due to the critical thickness and sensitivity values of soft

clay, the preliminary designs for soil stabilization should be considered before construction such as changing the slope geometry, reinforcing the slope, and installing supporting piles.

Acknowledgments

The authors would like to acknowledge King Mongkut's Institute of Technology Ladkrabang, Department of Rural Roads, University of Bengkulu, Tokai University, Suranaree University of Technology (SUT), and Thailand Science Research and Innovation (TSRI).

References

Abramson, L.W., Lee, T.S., Sharma, S. and Boyce, G.M. (2002), *Slope Stabilisation and Stabilisation Methods*, John Willey & Sons Inc.

Artidteang, S., Bergado, D.T. and Chaiyaput, S. (2013), "Stability analyses of embankment with limited life woven geosynthetics (LLGs) reinforced on soft clay", *Proceedings of the 18th Southeast Asian Geotechnical & Inaugural AGSSEA Conference*, Singapore, May.

ASTM D-2488 (2017), Description of identification of soils (visual-manual procedure). Annual Book of ASTM Standard. Philadelphia, PA, USA.

ASTM D-2573 (2018), Standard test method for field vane shear test in saturated fine-grained soils. Annual Book of ASTM Standard. Philadelphia, PA, USA.

Bergado, D.T., Chaiyaput, S., Voottipriex, P., Hino, T. and Chanmee, N. (2017), "Mitigations of flooding and soil erosions geo-disasters in Thailand and Laos due to climate change: from mountains to Lowlands", *Lowl Technol. Int.*, **19**(1), 63-76.

Bjerrum, L. (1972), "Embankments on soft ground", *Proceedings of the ASCE Conference on Performance of Earth-Supported Structures*, Purdue University, June.

Bow, V.L. (2019), "Incorporating geophysical data in slope stability modeling for two slopes in Arkansas", Graduate Theses and Dissertation, University of Arkansas, Fayetteville.

Chaiyaput, S., Bergado, D.T. and Artidteang, S. (2012), "FEM 2D numerical simulations reinforced embankment on soft ground by limited life geosynthetics (LLGs)", *Proceedings of the 5th Asian Regional Conference on Geosynthetics (GA2012)*, Bangkok, Thailand, December.

Chaiyaput, S., Bergado, D.T. and Artidteang, S. (2014), "Measured and simulated results of a kenaf limited life geosynthetics (LLGs) reinforced test embankment on soft clay", *Geotext Geomembranes*, **42**(1), 39-47. https://doi.org/10.1016/j.geotexmem.2013.12.006.

Chaiyaput, S. and Bergado, D.T. (2018), "Reconfirmation of Skempton-Bjerrum 2D to 3D settlement conversion using FEM of full scale embankments", *Lowl Technol. Int.*, **20**(1), 1-14.

Chaiyaput, S., Suksawat, T. and Ayawanna, J. (2021), "Evaluation of the road failure using resistivity and screw driving sounding testing techniques: A case study in Ang Thong province, Thailand", *Eng. Fail. Anal.*, **121**, 105171. https://doi.org/10.1016/j.engfailanal.2020.105171.

Chaiyaput, S., Sutti, N., Suksawat, T. and Ayawanna, J. (2022), "Electrical resistivity survey for evaluating the undrained shear strength of soft Bangkok clay at some of the canal-side road investigation sites", *Bull. Eng. Geol. Environ.*, **81**, 27. https://doi.org/10.1007/s10064-021-02537-3.

Dahlin, T. and Zhou, B. (2006), "Multiple-gradient array measurement for multichannel 2-D resistivity imaging", *Near Surf. Geophys.*, **4**(2), 113-123. https://doi.org/10.3997/1873-0604.2005037.

Department of Mineral Resources (2021), *Geological map*, [online]. Available from: http://www.dmr.go.th/download/pdf/Central_East/ayuttaya.pdf. [Accessed 5 January 2021].

Duncan, J.M., and Wright, S.G. (2005), *Soil Strength and Slope Stability*. John Wiley & Sons Inc.

Godio, A., Strobbia, C. and Bacco, G.D. (2006), "Geophysical characterisation of a rockslide in an Alpine region", *Eng. Geol.*, **83**, 273-286. https://doi.org/10.1016/j.enggeo.2005.06.034.

He, K., Ma, G., Hu, X., Liu, B. and Han, M. (2022), "The July 2, 2017, Lantian landslide in Leibo, China: mechanisms and mitigation measures", *Geomech. Eng.*, **28**(3), 283–298. https://doi.org/10.12989/gae.2022.28.3.283.

Hou, X.P., Chen, S.H. and Shahrour, I. (2021), "Judgement of rapid drawdown conditions in slope stability analysis", *Bull. Eng. Geol. Environ.*, **80**, 4379-4387. https://doi.org/10.1007/s10064-021-02253-y.

Jamsawang, P., Voottipruex, P., Jongpradist, P. and Likitlersuang, S. (2021), "Field and three-dimensional finite element investigations of the failure cause and rehabilitation of a composite soil-cement retaining wall", *Eng. Fail. Anal.*, **127**, 105532. https://doi.org/10.1016/j.engfailanal.2021.105532.

Kaufman, A.A. and Hoekstra, P. (2001), *Electromagnetic Soundings. Methods in Geochemistry and Geophysics*. Elsevier, Amsterdam.

Latha, G.M. and Garaga, A. (2010), "Stability analysis of a rock slope in Himalayas", *Geomech. Eng.*, **2**(2), 125-140. https://doi.org/10.12989/gae.2010.2.2.125.

Likitlersuang, S., Surarak, C., Wanatowski, D., Oh, E. and Balasubramaniam, A. (2013), "Finite element analysis of a deep excavation: a case study from the Bangkok MRT", *Soils Found*, **53**, 756-773. https://doi.org/ 10.1016/j.sandf.2013.08.013.

Loke, M.H. and Barker, R.D. (1996a), "Rapid least-squares inversion of apparent resistivity pseudosections by a quasi-Newton method", *Geophys. Prospect*, **44**(1), 131-152. https://doi.org/10.1111/j.1365-2478.1996.tb00142.x.

Loke, M.H. and Barker, R.D. (1996b), "Practical techniques for 3D resistivity surveys and data inversion", *Geophys. Prospect*, **44**(3), 499-523. https://doi.org/10.1111/j.1365-2478.1996.tb00162.x.

Lundström, K., Larsson, R. and Dahlin, T. (2009), "Mapping of quick clay formations using geotechnical and geophysical methods", *Landslides*, **6**, 1-15. https://doi.org/10.1007/s10346-009-0144-9.

Neoh, C.A. (2009), "Slope stabilization and protection for residential development profile", *Proceedings of the Conference on Landslide Risk Mitigation and Hillslope Re-engineering Planning*, PWTC Kuala Lumpur.

New Zealand Geotechnical Society (2005), *Guidelines for the field classification and description of soil and rock for engineering purposes*, New Zealand Geotechnical Society.

Orense, R.P., Mirjafari, Y. and Suemasa, N. (2019), "Screw driving sounding: a new test for field characterization", *Geotech. Res.*, **6**(1), 28 -38. https://doi.org/10.1680/jgere.18.00024.

Prabhakar, C. and Deshpande, R.A. (2014), "Evaluation of soil resistivity and design of grounding system for hydroelectric generating station in a hilly terrain — A case study", *Proceedings of the International Conference on Advances in Energy Conversion Technologies (ICAECT)*, Manipal. https://doi.org/10.1109/ICAECT.2014.6757070.

Rao, P., Wu, J., Jiang, G., Shi, Y., Chen, Q. and Nimbalkar, S. (2021), "Seismic stability analysis for a two-stage slope", *Geomech. Eng*, **27**(2), 189-196. https://doi.org/10.12989/gae2021.27.2.189.

Song, K., Yan, E., Zhang, G., Lu, S. and Yi, Q. (2015), "Effect of hydraulic properties of soil and fluctuation velocity of reservoir water on landslide stability", *Environ. Earth. Sci.*, **74**, 5319-5329. https://doi.org/10.1007/s12665-015-4541-1.

Sun, G., Yang, Y., Jiang, W. and Zheng, H. (2017), "Effects of an increase in reservoir drawdown rate on bank slope stability: a case study at the Three Gorges Reservoir, China", *Eng. Geol.*, **221**, 61-69.

https:// doi.org/10.1016/j.enggeo.2017.02.018.
Tran, A.T.P., Kim, A.R. and Cho, G.C. (2019), "Numerical modeling on the stability of slope with foundation during rainfall", *Geomech. Eng.*, **17**(1), 109-118. https://doi.org/10.12989/gae.2019.17.1.109.
Udomchai, A., Hoy, M., Horpibulsuk, S., Chinkulkijniwat, A. and Arulrajah, A. (2018), "Failure of riverbank protection structure and remedial approach: A case study in Suraburi province, Thailand", *Eng Fail. Anal.*, **91**, 243-254. https://doi.org/10.1016/j.engfailanal.2018.04.040.
Viberg, L. (1984), "Landslide risk mapping in soft clays in Scandinavia and Canada", *4th International symposium on landslides*, Toronto.
Wang, L. and Zhang, G. (2014), "Centrifuge model test study on pile reinforcement behavior of cohesive soil slopes under earthquake conditions", *Landslides*, **11**(2), 213-223. https://doi.org/10.1007/s10346-013-0388-2.
Zhang, S.L., Yin, Y.P., Hu, X.W., Wang, W.P., Li, Z.L., Wu, X.M., Luo, G. and Zhu, S.N. (2021), "Geo-structures and deformation-failure characteristics of rockslide areas near the Baige landslide scar in the Jinsha River tectonic suture zone", *Landslides*, https://doi.org/10.1007/s10346-021-01741-2.

CC